Crack detection in photovoltaic cells using electronic speckle pattern interferometry

Tzu-Kuei Wen, Ching-Chung Yin
Department of Mechanical Engineering, National Chiao Tung University
Hsinchu, Taiwan, R.O.C.

ABSTRACT

This paper presents a full field nondestructive testing method to inspect the micro-defects embedded in photovoltaic (PV) cells by using electronic speckle pattern interferometry. The edge-clamped solar cells were heated to induce thermal deflection. Interference fringe enhanced by speckle patterns correlated to thermal deformation were determined by subtraction of two pictures recorded at different temperatures and image processing technique based on Fourier optics. The interference fringes produced at the defect free specimen exhibit a number of polygons with regular patterns of bright and dark fringes which are concentric with the center of the specimen. The thermal deformation will be redistributed due to appearance of the defects. The heating-induced interference fringes become quite different from those of the undamaged one. Tangential discontinuities of interference fringes or locally concentric polygon patterns occur in the contiguous area around the micro-defects or damages. The application of large temperature gradient to silicon substrates will induce crack propagation and should be prevented in ESPI inspection.

Keyword: silicon-based photovoltaic cell, electronic speckle pattern interferometry, micro-defect, thermal deformation

1. INTRODUCTION

Micro-defects are frequently generated in silicon-based solar cell substrates during fabrication. Optical inspection for very thin cracks is extremely time-consuming. These defects usually result in catastrophic damages when the brittle silicon substrates are manufactured in module process. They also cause the solar cells breaking down in service. Micro-defects detection is an important issue in quality control of silicon substrates or solar cells. Manufacturers can raise quality and avoid wasting cost if those damages could be detected in silicon/solar cells before being packaged. Recently, there are a number of experimental techniques and approaches used for defect detection in silicon substrates and solar cells for fast growing PV industry. These include photoacoustic methods [1-3], optical image process captured from the silicon/solar cells by CCD (charge-coupled device) camera [4], resonance ultrasonic vibration (RUV) method by applying ultrasonic vibrations of tunable frequency and adjustable amplitude to specimens [5-6], photoluminescence (PL), and electroluminescence (EL) methods [7-8]. Each method has individual advantages such as detection for the size, location of defects, etc. However, there is no inspection method which can examine for micro-defects in the whole cell not only rapidly but precisely for PV industry up to the present.

In this paper, we present a rapid inspection method using electronic speckle pattern interferometry (ESPI) to detect both the size and location of micro-defects in solar cells. ESPI is widely known and used for full field, non-destructive inspection and deformation measurements. Speckle patterns would be induced while the light was scattered by the rough surface of the object. ESPI is based on the slight changes in the scattered speckles determined by electronically subtracting the speckle patterns before deformation from those captured after deformation happened in the object [9]. ESPI has been applied to measure heating-induced deflection of the specimen [10-12]. The displacement discontinuity might occur on opposite sides of a crack under strains. The discontinuity results that speckle fringes have distinct tangential slopes across the crack interface. The speckle fringes regarding heating-induced deformation in the solar cells with defects will have different patterns rather than those free of damages. Evidence from the discontinuous tangential slopes of speckle fringes significantly raises the probability of micro-defect detection in solar cells. The variation of speckle fringes can be used to determine the size and location of micro-defects.

Fourth International Conference on Experimental Mechanics, edited by C. Quan, K. Qian, A. Asundi, F. S. Chau,
Proc. of SPIE Vol. 7522, 75224Q · © 2010 SPIE · CCC code: 0277-786X/10/$18 · doi: 10.1117/12.851695

Downloaded From: http://proceedings.spiedigitallibrary.org/ on 04/25/2014 Terms of Use: http://spiedl.org/terms

2. OUT-OF-PLANE ESPI

The schematic view of out-of-plane ESPI setup is shown in Figure 1. This optical measurement system is the same as Michelson interferometer. The laser beam passing through spatial filter and beam splitter was used to illuminate the specimen and the reference plane. The reflected beams from the specimen and reference plane come across the beam splitter again and captured by CCD camera. The signal from CCD camera was then recorded by a personal computer.

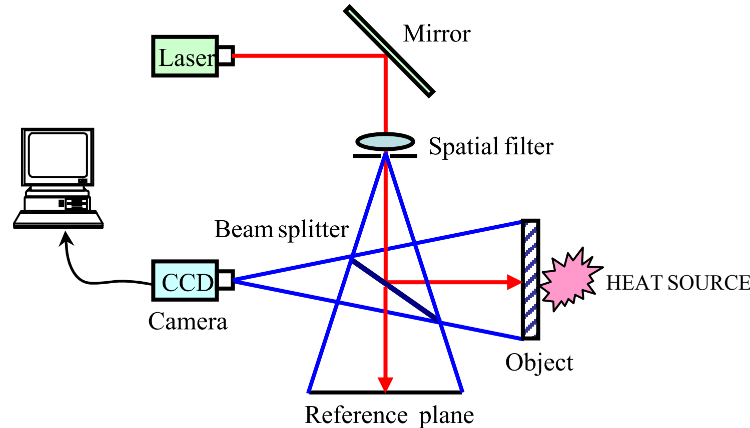

Figure 1. Out-of-plane displacement measurement by ESPI

The intensity distribution at any point of the undeformed object can be expressed as

$$I_1 = \mathbf{u}_o^2 + \mathbf{u}_r^2 + 2\mathbf{u}_o\mathbf{u}_r \cos(\phi_o - \phi_r) \tag{1}$$

where $\mathbf{u}_o, \mathbf{u}_r, \phi_o, \phi_r$ are the randomly varying amplitude and phase at a point on the object and reference plane. If a deformation is produced at the object by mechanical load or thermal stress, the intensity distribution of light reflected from the deformed object is given by

$$I_2 = \mathbf{u}_o^2 + \mathbf{u}_r^2 + 2\mathbf{u}_o\mathbf{u}_r \cos(\phi_o - \phi_r + \delta) \tag{2}$$

where δ is the phase change introduced due to the deformation of object. These two intensity distributions are recorded in CCD camera and digitized in computer that converted to amplitude transmittance upon processing.

$$\begin{aligned} I_{total} &= I_2 - I_1 \\ &= 2\mathbf{u}_o\,\mathbf{u}_r\left[\cos(\phi_o - \phi_r + \delta) - \cos(\phi_o - \phi_r)\right] \\ &= 4\,\mathbf{u}_o\,\mathbf{u}_r \sin\left(\phi_o - \phi_r + \frac{\delta}{2}\right)\sin\left(\frac{\delta}{2}\right) \end{aligned} \tag{3}$$

Eq. (3) comprises two terms. The first term, $\sin(\phi_o - \phi_r + \delta/2)$, is a higher-frequency modulation. The high spatial frequency speckle noise was eliminated by using the image processing technique based on Fourier optics. The second term, $\sin(\delta/2)$, is a low-frequency modulation varying between -1 and 1. The positive value of $\sin(\delta/2)$ indicates brightness on the image. The brightness will be zero when $\delta = 2m\pi$; $m = 0, \pm 1, \pm 2,$ etc. The correlated speckles display bright or dark fringes as a result of the phase difference. The phase difference depends only on the out-of–plane displacement component d_z and the bright fringes are formed [13].

$$d_z = \frac{m\lambda}{2} \tag{4}$$

Downloaded From: http://proceedings.spiedigitallibrary.org/ on 04/25/2014 Terms of Use: http://spiedl.org/terms

3. EXPERIMENT RESULTS

The polycrystalline Si solar cells were used as specimens. Their sizes were 125 × 125 ×0.2 and 175 × 175 × 0.2 mm. One surface of the specimen was coated by anti-reflection film of thickness about 0.015 mm and spread with the regular electrode pattern. The other surface had texturization and two major tin strips having a size of 125 × 4 × 0.01 mm. The edge-clamped solar substrates were heated to induce deflection and generated speckle fringe patterns by using the out-of-plane ESPI. A temperature controllable planar heater was used to provide heat flux to the object as shown in Figure 1. A series of the specklegrams were captured every constant temperature increment by CCD camera, which was controlled by LabVIEW program. Thermal loading was induced by heating the illuminated surface of the specimen. The heater temperature was measured by J-type thermocouple through a module NI-9213, and displayed on PC. The illuminating source was a DPSS laser at a wavelength of 532 nm. According to Eq. (3), the increment of contour was 266 nm. The whole specimen surface was illuminated by an expanded laser beam through a spatial filter. A high-resolution CCD camera of 2448 × 2050 pixels was utilized. A couple of specimens were tested. Each had very a thin edge crack which was artificially made by pressing a small pyramid shaped diamond indenter under a Matsuzawa digital rockwell hardness tester. An eraser is used to knock at the small crack to induce crack propagation from its center location. Figure 2 shows the photo of a crack observed by Axioskop 40 POL microscope. The crack length was about 70 mm, and its width was less than 0.005 mm.

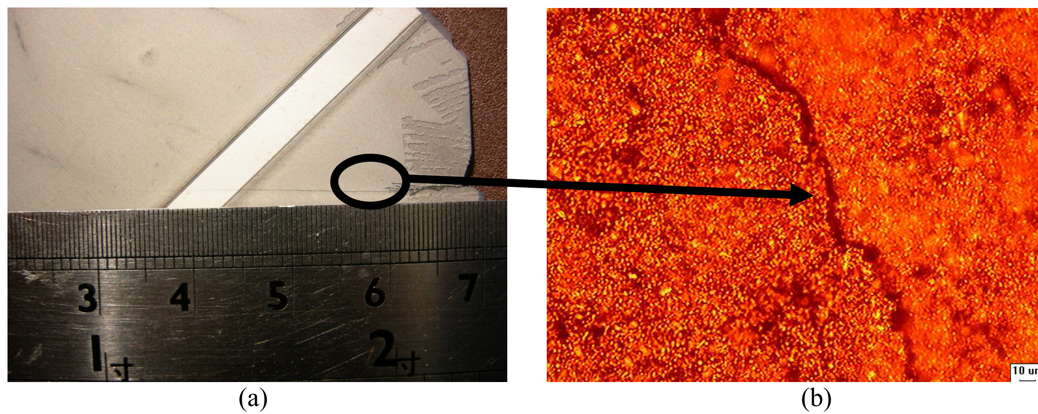

(a) (b)

Figure 2. (a) The visual length of a diagonal edge crack is about 70mm. (b) The width of the crack is less than 5 μm, measured by Axioskop 40 POL microscope.

4. DISCUSSIONS

Figure 3(a) shows the out-of-plane ESPI image of a undamaged solar cell. A number of displacement fringes reveal that initial out-of-plane bending deformation appears in the cell because tin-strips and silicon substrate have different coefficients of thermal expansion. Every point in the same fringe has the same out-of-plane displacements in this specimen. Figure 3(b) depicts the interference fringes regarding out-of-plane deformation for a cell with a small artificially made edge defect. The tangential slopes of displacement fringes are discontinuous across the edge crack which appears inside the solid-line circle.

Figure 4 shows the interference fringes recorded for the defect free specimen in temperature ranges of ΔT and $2\Delta T$, respectively. The speckle pattern exhibits a number of polygons with regular patterns of bright and dark fringes which are concentric with the center of the specimen. The shape of polygon speckle pattern depends on specimen constraints. The number of fringes is increased due to large temperature increment applying to the specimen. The fringes indicate out-of-plane displacements of the specimen. The maximum displacement was generated in the center of the specimen. Those points located on each fringe possess the same magnitude of displacement. The number of ESPI fringes shown in Figure 3(b) is about twice of that in Figure 3(a) because of double temperature increment.

Figure 5 reveals speckle fringes of the specimen with an edge defect shown in Figure 2. The fringe patterns for defect free specimen shown in Figure 4 are quite different from those in Figure 5. Two major differences between these ESPI

Downloaded From: http://proceedings.spiedigitallibrary.org/ on 04/25/2014 Terms of Use: http://spiedl.org/terms

fringe patterns are found. Firstly, the tangential slopes of contiguous speckle fringes are discontinuous across the crack interface. The uniformity of heat flux transferred from planar heater to the specimen was changed due to the diagonal edge crack in the specimen. It causes the discontinuous displacements at opposite sides of the defect. Secondly, locally

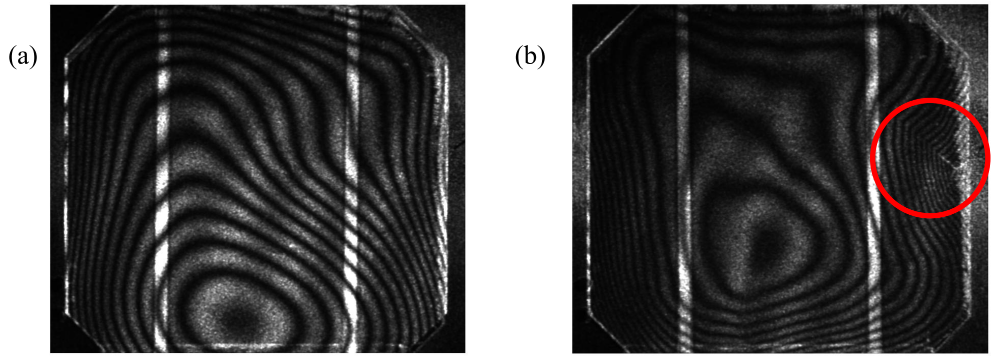

Figure 3. The out-of-plane ESPI image of a solar cell without damage (a) and the same cell damaged with an edge defect appearing inside the circle (b).

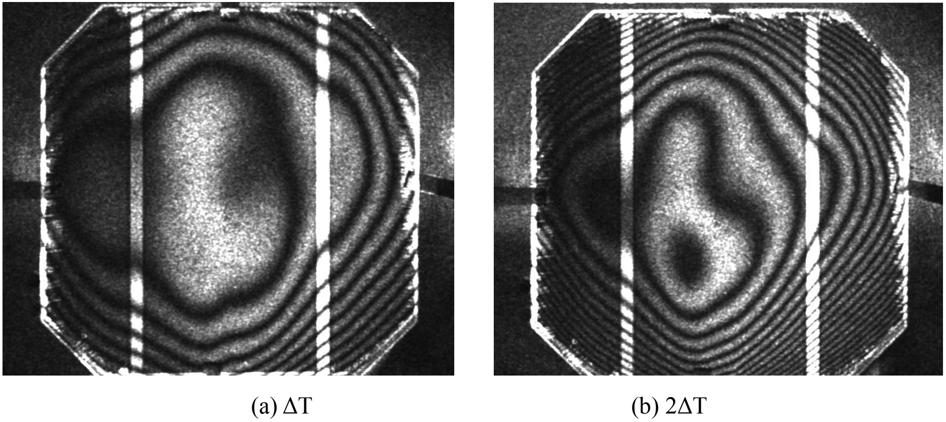

(a) ΔT (b) 2ΔT

Figure 4. The interference fringes were measured in defect free specimen under deferent temperature changes.

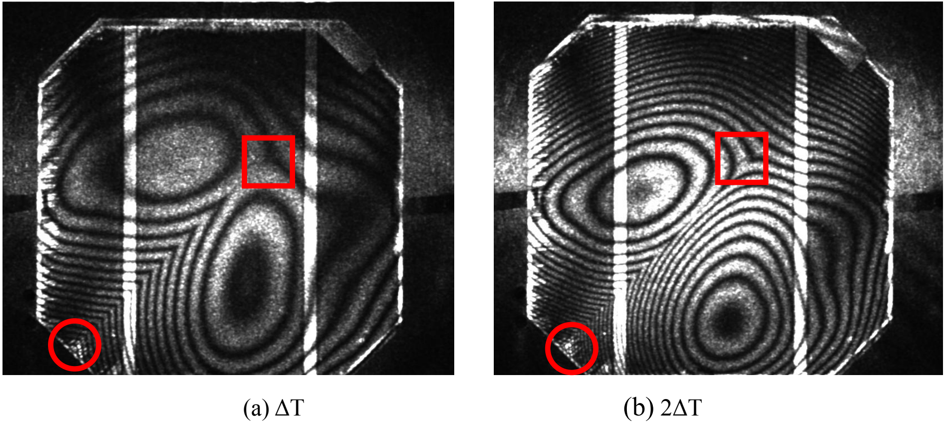

(a) ΔT (b) 2ΔT

Figure 5. The interference fringes were recorded for the specimen with defects at different temperature changes. The mark circular and rectangular regions are the initiating point and arrest point of crack extension, respectively.

Downloaded From: http://proceedings.spiedigitallibrary.org/ on 04/25/2014 Terms of Use: http://spiedl.org/terms

concentric polygons are divided into two fringe systems in the central region of specimen by the crack. In addition, the crack shown in Figure 2(a) is over the half diagonal length of the specimen (76 mm), which is longer than the visual length 70 mm. The thermal deflection was redistributed over the whole specimen. The second phenomenon observed in the specimen was caused by the non-homogeneous heating-induced deformation. The new maximum displacement would be removed and its location depends on the crack extension and various constraint conditions. The number of fringes in adjacent locally concentric polygons might be different. Optical inspection for a very thin micro-defect in the solar cell is very time-consuming. However, a clear recognition of the heating-induced speckle patterns provides us an effective and rapid inspection for micro-defects in solar cells.

5. CONCLUSIONS

This paper presents a full field nondestructive inspection for micro-defects embedded in PV cells by using ESPI. To achieve consistent conclusion, we have confirmed that each defect-free specimen had the similar speckle patterns under the same constraints, temperature increment, etc. If the specimen had micro-cracks or defects, the interference fringes regarding heating-induced deflection would be different from the undamaged one. The fringe pattern for solar cell produced by laser speckle could be useful to diagnose size and location of very thin micro-cracks.

Only edge defects were considered in this work. The defects were made artificially by a small pyramid-shaped diamond indenter. It is found that the speckle fringes for a small crack are not continuous across the edge crack. It indicates the displacements are not continuous across the crack surface. The fringes in the front of crack tip appear with discontinuous tangential slopes. It could be used to characterize the crack length. In addition, the interference fringes on the opposite sides of a long crack have their own individual concentric fringes.

REFERENCES

1. Mikoshiba, N., Nakamura, H., and Tsubouchi, K., “Photoacoustic measurement of nonradiative lifetime and defect in silicon wafers,” *Jpn. J. Appl. Phys.*, 23, 685-690 (1984).
2. Kasai, M., Shimizu, H., Sawada, T., and Gonhshi, Y., “Non-destructive observation of stacking faults of silicon-wafer by means of photoacoustic Microscopy,” *Analytical Sciences*, 1, 107-109 (1985).
3. Berquez, L., Marty-Dessus, D., and Franceschi J. L., “Defect detection in silicon wafer by photoacoustic imaging,” *Jpn. J. Appl. Phys.*, 42, 1198-1200 (2003).
4. Fu, Z., Zhao, Y., Liu, Y., Cao, Q., Chen, M., Zhang, J., and Lee, J., “Solar cell crack inspection by image processing,” *Proc. Int. IEEE Conf. Business of Electronic Product Reliability and Liability*, Shanghai, China, 77-80 (2004).
5. Belyaev, A., Polupan, O., Dallas, W., Ostapenko, S., Hess, D., and Wohlgemuth, J., “Crack detection using resonance ultrasonic vibrations in full-size crystalline silicon wafers,” *Appl. Phys. Lett.*, 88, 111907(2006).
6. Belyaev, A., Polupan, O., Dallas, W., Ostapenko, S., Hess, D., and Kalejs, J. P., “Resonance ultrasonic vibration diagnostics of elastic stress in full-size silicon wafers,” *Semicond. Sci. Technol.*, 21, 254-260(2006).
7. Trupke, T., Bardos, E. A., Schubert, M. C., and Warta, W., “Photoluminescence imaging of silicon wafers,” Appl. Phys. Lett., 89, 044107 (2006).
8. Fuyuki, T., Kondo, H., Yamazaki, T., Takahashi, Y., and Uraoka, Y., “Photographic surveying of minority carrier diffusion length in polycrystalline silicon cells by electroluminescence,” *Appl. Phys. Lett.*, 86, 262108 (2005).
9. Meinlschmidt, P., Hinsch, K. D., Sirohi, R. S., and Thompson, B. J., [Electronic Speckle Pattern Interferometry Principle and Practice], SPIE Optical Engineering Press (1996)
10. Chiang, F. P., Anastasi, R., Beatty J., and Adachi, J., “Thermal strain measurement by one-beam laser speckle interferometry,” *Applied Optics*, 19, 2701-2704 (1980).
11. Hack E.; Bronnimann R., “Electronic speckle pattern interferometry deformation measurement on lightweight structures under thermal load,” Optics and Lasers in Engineering, 31(3), 213-222 (1999).
12. Zarate, E. A., Custodio, E. G., Trevino-Palacios, C. G., Rodriguez-Vera, R., and Puga-Soberanes, H. J., “Defect detection in metals using electronic speckle pattern interferometry,” *Solar Energy Materials & Solar Cells*, 88, 217-225 (2005).
13. Sirohi S. and Chau, F. S., [Optical Methods of Measurement: Wholefield Techniques], Marcel Dekker, Inc, New York & Basel, 127-182 (1999).

Downloaded From: http://proceedings.spiedigitallibrary.org/ on 04/25/2014 Terms of Use: http://spiedl.org/terms